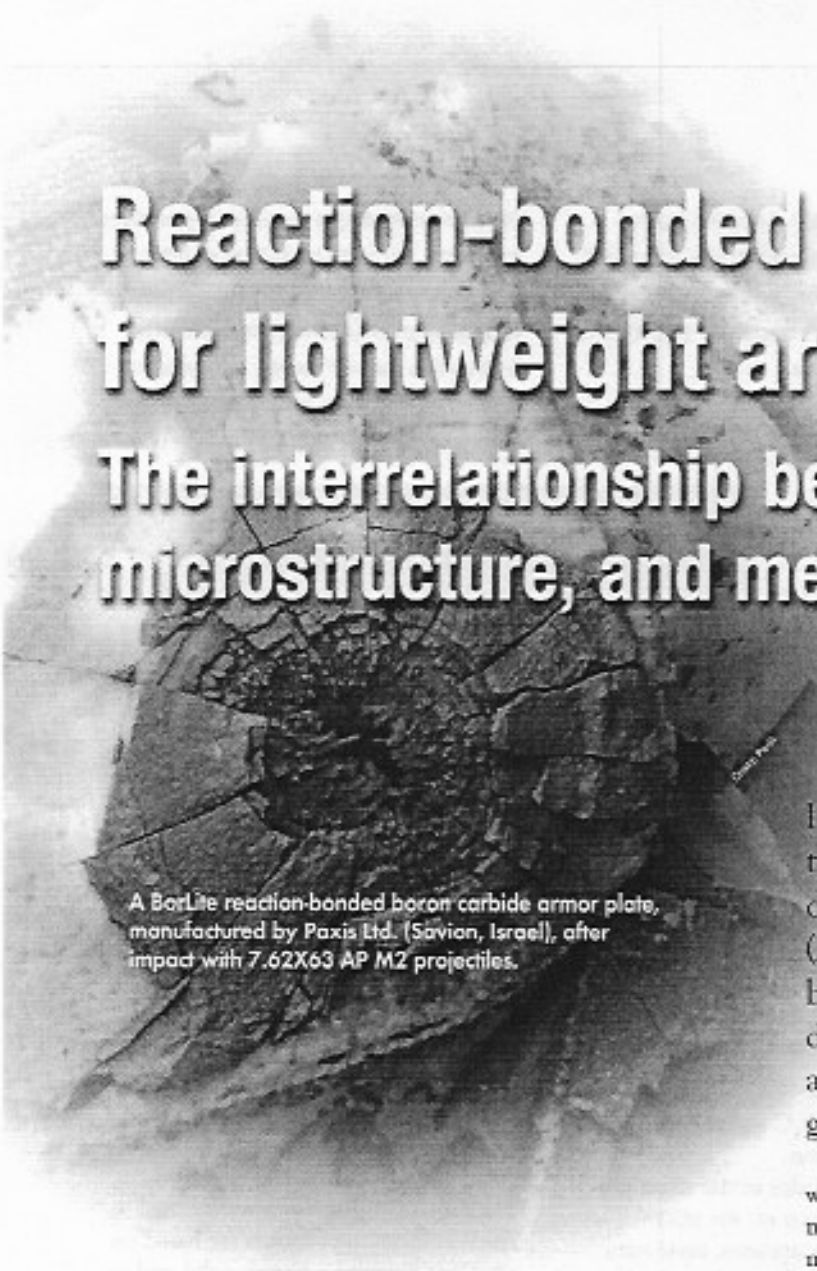
Reaction-bonded boron carbide for lightweight armor:

The interrelationship between processing, microstructure, and mechanical properties



A BorLite reaction-bonded boron carbide armor plate, manufactured by Paxis Ltd. (Savion, Israel), after impact with 7.62X63 AP M2 projectiles.

By Shmuel Hayun

With adequate understanding of processing parameters and resulting material properties, reaction bonding offers a relatively inexpensive alternative fabrication method for lightweight ceramic armor.

Since the dawn of history, weapons and armor have been in a life-and-death struggle. During the last three decades of the 20th century, a variety of ceramics, including aluminum nitride (AlN), aluminum oxide (Al_2O_3), boron carbide (B_4C), silicon carbide (SiC), titanium diboride (TiB_2), tungsten carbide (WC), and zirconium oxide (ZrO_2), were investigated as armor materials.

Light ceramics particularly are attractive for personnel as well as land and airborne vehicle protection. The most commonly used ceramics are Al_2O_3, SiC, and B_4C. Al_2O_3 is the most economical alternative, but its final protection solutions are heavier, because Al_2O_3 has the highest density and lowest ballistic efficiency of the three light ceramics. B_4C is the hardest ceramic, but it undergoes an amorphization process at high impact pressures (such as with WC-cored bullets), which weakens the armor. Although SiC has no amorphization issues, its higher density (3.2 g/cm^3) compared with B_4C (2.52 g/cm^3) limits its use.

We must consider some other points when choosing an adequate armor material. For instance, low porosity in the ceramic tile generally results in better ballistic performance. Moreover, smaller grain sizes increase ballistic performance. In addition, ease of fabrication and cost are of paramount importance in considering a particular material for armor applications. Full density of B_4C or SiC is a prerequisite for achieving acceptable ballistic resistance, but can be attained only by hot-pressing fine powder (<2 μm) in the presence of sintering additives at relatively high temperatures (>2,473 K). Further, production method strongly affects properties of the ceramic: hot-pressing tiles often results in a harder ceramic, which is optimal against a single hit, whereas reaction-bonding tiles provide better multihit performance. However, there is no

Capsule summary

THE POTENTIAL

Reaction-bonding fabrication methods offer a low-cost route to produce composites with effective ballistic impact resistance, generating materials with great potential for lightweight armor applications.

THE CAVEAT

Despite the potential of reaction-bonded materials for armor applications, processing variables in reaction-bonding techniques can significantly reduce mechanical properties of resulting composites.

THE SOLUTION

Better understanding of the effect of processing parameters on the microstructure of infiltrated composites, their static and dynamic mechanical properties, and microstructure–property relationships can help develop more efficient reaction-bonded boron carbide for lightweight armor applications.

clear correlation between quasi-static and/or dynamic mechanical properties and the ballistic behavior of ceramics. Nonetheless, some parameters, such as hardness, fracture toughness, and elastic modulus, are expected to have an influence.

Elevated hardness values are, by common consensus, crucially important for good ballistic resistance, because a material with sufficiently high hardness deforms or fragments a projectile upon impact.[1] Moreover, ceramic fragments may continually abrade the projectile during the rest of the penetration process.[2] It is, however, unclear if harder is always better, because one of the main failure modes of thin ceramic tiles is related to fracture from tensile stresses, which higher hardness does not improve.

Competition between high performance of carbide ceramics and the high cost of conventional fabrication methods led to the development of relatively inexpensive alternative fabrication methods capable of providing adequate mechanical properties. One approach is based on the reaction-bonding technique. According to this approach, ceramic powder (SiC, B_4C, or B_4C–SiC mixture) is mixed with free carbon, compacted, and subsequently infiltrated with molten metal (e.g., silicon or aluminum alloys). Molten metal reacts with free carbon and with carbon that originates in B_4C to form a ceramic composite. The resulting composite has high cohesive strength and elevated hardness values and is an effective ballistic impact-resistant material. Several variants of reaction-bonding processes, as well as the properties of final composites, are described in scientific journals and in patents.

One crucial drawback associated with reaction-bonded composites, however, is the fraction of the residual metal/alloy that significantly reduces the composite's mechanical properties. This fraction strongly depends on initial porosity of the preforms and on the fraction of additional free carbon. Several approaches can reduce initial preform porosity, including partial sintering, use of multimodal powder mixtures, addition of elements that react with the alloy/metal to form stable phases, and addition of elements (e.g., titanium or iron) or compounds (e.g., TiC) that react with B_4C and release additional free carbon.

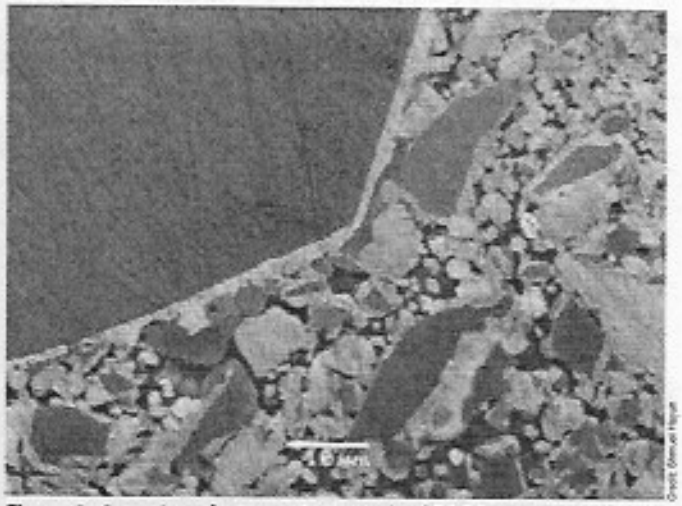


Figure 1. Scanning electron micrograph of RBSC composite. The new SiC layer (white color) precipitates on initial SiC particles (darker color).

Thus, knowledge of the effect of processing parameters on the microstructure of infiltrated composites, their static and dynamic mechanical properties, and microstructure–property relationships is necessary to understand and develop more efficient armor.

Processing of reaction-bonded composites

Reaction bonding is a special case of reaction-forming processes that represent an important alternative to conventional sintering processes, such as solid-state sintering, liquid-phase sintering, and hot pressing. For polycrystalline ceramics fabricated by processes involving chemical reactions, consolidation between constitutive particles occurs by formation of new phases rather than by a neck-growth mechanism induced by relatively weak surface energy forces. In general, these processes have the advantage of reducing working temperature, shaping materials in potentially complex and large near-net shapes, and reducing or even canceling postconsolidation machining. All these make the reaction-forming process an obvious direct cost–benefit method. The most important and widely used reaction-forming processes are based on reactions between a porous solid and an infiltrating liquid phase.

Reaction-bonded silicon carbide (RBSC) composites

The reaction-bonding approach was first suggested and developed in the 1950s for SiC.[3] According to this approach, a porous body (preform) consisting of the ceramic phase and free carbon is infiltrated with liquid silicon, which reacts with the carbon to form a secondary SiC phase. The resulting microstructure (Figure 1) consists of original SiC particles surrounded by a secondary SiC phase and 5–15 vol% of residual silicon.[4] Pre-existing, primary SiC particles are bonded by the newly formed SiC phase. A recent spin-off that uses diamond as a carbon source shows huge potential—the new composites show elevated stiffness, hardness, and thermal conductivity values.

The microstructure and mechanical properties of RBSC have been thoroughly investigated. Previous studies established the effect of compacted preform properties (porosity, pore size and distribution, fraction of free carbon, and carbon source) and processing parameters (temperature and duration of the infiltration procedure as well as cooling regime) on the microstructure of infiltrated composites and their mechanical properties.[5]

RBSC materials display high mechanical properties, including hardness (15–25 GPa), Young's modulus (320–400 GPa), flexural strength (100–400 MPa), and fracture toughness (~3.9 MPa-$m^{1/2}$).[6] Two main factors determine mechanical properties of an RBSC:

- Fraction of residual silicon, the properties of which are significantly lower than those of the SiC phase; and
- Structure and strength of the interfaces between RBSC phases.

The first factor is straightforward—we can reduce the fraction of residual silicon by adding reactive elements to the silicon melt. These elements react with residual liquid silicon to form silicide phases. The second factor is more complex and is discussed widely in the literature. Reported results regarding the nature of Si/SiC and α-SiC/β-SiC interfaces are summarized in a review by Ness and Page,[7] who conclude that occasional misfit dislocations and steps are formed at Si/SiC interfaces. These observations are in good agreement with the results of Naylor and Page,[8] who show that the Si/SiC interface is mechanically weak and provides a preferential path for fracture under indentation. Interfaces between β-SiC and α-SiC are semicoherent, and it is suggested that SiC/SiC α/α, α/β, β/α and β/β) grain boundaries are strongly bonded by a thin layer (~1 nm) of amorphous SiC.

Reaction-bonded boron carbide (RBBC) composites

In 1973, Taylor and Palicke[9] submitted a patent on "Dense carbide composite for armor and abrasives." In this patent and other papers, Taylor and Palicke touch upon several key issues of the process that recurrently is referred to in subsequent patents. The authors fabricated dense carbide composites using the same technique for RBSC, but, instead of SiC, they used B_4C. They discuss issues, including the source of the carbon that is meant to react with molten silicon (which may be a free-carbon addition), a carbon-based binder (which provides minimal self-supporting strength to the green body), or B_4C itself (which releases carbon when in contact with molten silicon). Taylor and Palicke also discuss the importance of B_4C particle-size distribution and its effect on efficient volume filling. The authors argue that at least 12 vol% of residual silicon is necessary to achieve good fabrication yields (i.e., composites without cracks). This requirement puts a major drawback on RBBC, similar to RBSC, where residual silicon creates soft spots that detract from overall ballistic efficiency of the product. Since then, the research has expanded to overcome this obstacle and to reduce the amount of residual silicon in RBSC.

Table 1. Technological parameters of specimen fabrication

Specimen	Initial particle size (μm)	Partial sintering, 30 min	Carbon addition	Alloying elements	Porosity of preform (vol%)
RB	1, 5, 100	No	No	No	30, 45
RBM	Multimodal powder mixtures[†]	No	No	No	25
RI	1, 5	2,173–2,373 K	No	No	20, 30, 40
RIC	1, 5	2,173–2,373 K	Yes	No	20, 30, 40
RITC[‡]	1, 5	2,343–2,403 K	No	TiC	20, 30, 40
RIFE[§]	5	2,273 K	No	Fe	30

[†]Powder mixtures consists of 60, 15, and 25 parts of particles with average sizes of 106, 13, and 1 μm.
[‡]RITC is reaction infiltration of partly sintered B_4C–TiC body infiltrated with carbon.
[§]RIFE is reaction infiltration of partly sintered B_4C–Fe body infiltrated with silicon

Fabrication approaches for RBBC composites

The fraction of residual silicon strongly depends on initial porosity of the preforms and on initial fraction and distribution of free carbon within a compacted body. To reduce initial porosity of the preforms, we can either partly sinter B_4C compacts to a desired porosity or use a mixture of optimally distributed B_4C powders of various average particle sizes.

At early stages of our work, we realised that use of resins as a source of free carbon should be avoided, because toxic gases are released during pyrolysis. Thus, we used several alternative methods, including pyrolysis of commercial sugar after drying a 50:50 water solution and addition of carbon content (TiC) or carbon release elements (iron) to B_4C, where the reaction between these compounds releases free carbon. Technological parameters for specimen fabrication are presented in Table I.

Microstructure and phase composition of B_4C composites

Studies establish the microstructure and phase composition of silicon-infiltrated B_4C composites fabricated via various approaches. The following phase compositions were studied:

- Reaction-bonded (RB, green B_4C body infiltrated with silicon);
- Reaction-bonded multimodal (RBM, green B_4C body made of multimodal particles infiltrated with silicon;
- Reaction-infiltrated (RI, partly sintered body infiltrated with silicon); and
- Reaction-infiltrated with added carbon (RIC, partly sintered body with added free carbon and infiltrated with silicon).

These materials consist of four phases: original B_4C particles; ternary $B_{12}(B,C,Si)_3$ compound; β-SiC; and residual silicon (Figure 2). The reaction between molten silicon and B_4C particles results in core–rim structure formation and a β-SiC phase of single platelike particles.

Aghajanian et al.[10] stress that the reaction of molten silicon with B_4C has a deleterious effect and suggest the use of boron as an alloying element to silicon to curtail its interaction with the ceramic matrix. However, thermodynamic analysis and experimental results show that formation of the silicon-containing B_4C compound $B_{12}(B,C,Si)_3$ during the RBBC process is independent of the fabrication approach and always occurs in the B-C-Si system. Results from

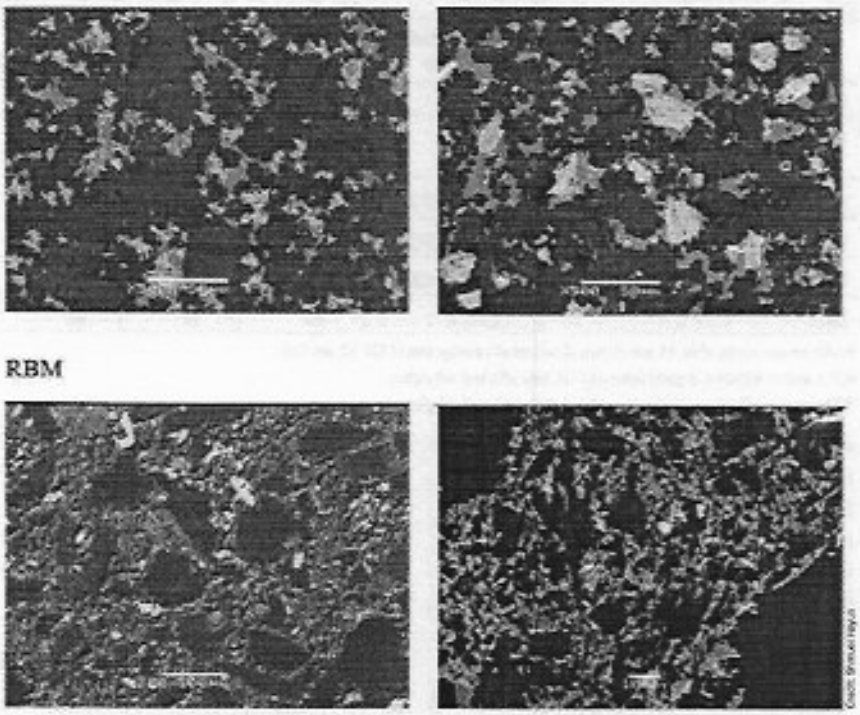


Figure 2. Scanning electron micrographs of bulk regions in RI, RIC, and RBM composites. In RBM composite, left image shows microstructure after removal of residual silicon; right image shows enlarged area between two large B_4C grains.

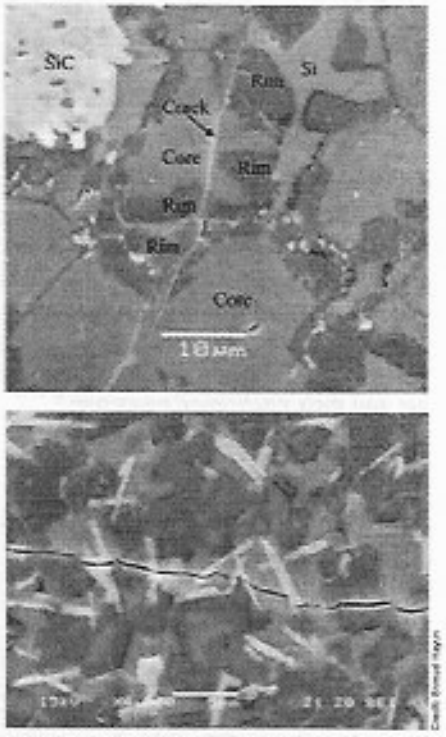


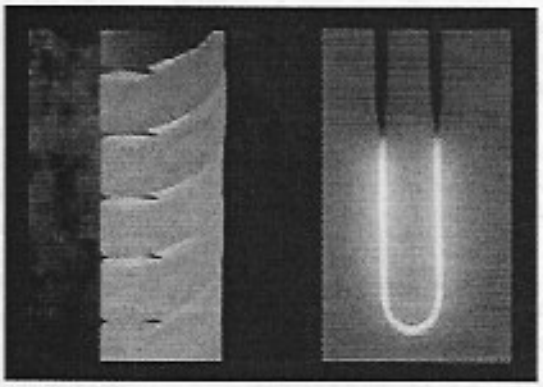
Figure 3. Crack propagation path in the composite underlines strength of the boundary between the B_4C particle core and adjacent rim. Moreover, interaction with SiC plates causes multiple crack deflections.

nanoindentation experiments show that average hardness and Young's modulus values of the $B_{12}(B,C,Si)_3$ phase (H_V = 46.1 + 4.2 GPa and E = 474 + 34 GPa, respectively) are slightly higher than those of the initial B_4C phase (H_V = 42.0 + 3.3 GPa and E = 460 + 23 GPa).[11] In addition, inspection of a crack propagation path indicates that the boundary between core and rim regions is relatively strong and does not deflect the propagating crack (Figure 3). Thus, the newly formed $B_{12}(B,C,Si)_3$ phase does not reduce mechanical properties of the composite.

The mechanism of core–rim structure formation is attributed to the dissolution precipitation process, which is well accounted for by thermodynamic analysis of the B-C-Si system.[12] Because B_4C is a covalently bonded solid, its components diffuse at an extremely low rate, and, therefore, it dissolves congruently (i.e., with no compositional changes). Boron concentration in the melt as a result of congruent dissolution is 8.0 at.% of boron. At the same time, boron content in the melt, which is in equilibrium with SiC and the ternary $B_{12}(B,C,Si)_3$ phase, is ~6.6 at.%. Thus, congruent dissolution of B_4C provides the required oversaturation for ternary carbide formation, and precipitation of the $B_{12}(B,C,Si)_3$ phase establishes overall equilibrium conditions in the system. Precipitation of the ternary carbide phase takes place at the interface of original B_4C particles and leads to formation of rim regions. The dissolution–precipitation process continues as long as the liquid is in contact with original B_4C particles.

The amount of various phases within RBBC composites is strongly affected by two factors, neither of which is free-carbon addition (Table 2). The first and obvious factor is initial porosity of the preforms, which determines amount of residual silicon and

Starbar *and* **Moly-D** elements
are *made in the U.S.A.*
with a focus on providing
the highest quality heating elements
and service to the global market.



I²R -- 50 years of service and reliability

I Squared R Element Co., Inc.
Akron, NY Phone: (716)542-5511
Fax: (716)542-2100
Email: sales@isquaredrelement.com
www.isquaredrelement.com

Table 2. Average phase distribution in carbon-free and carbon-containing composites

Material	Initial porosity	B_4C (vol%)	SiC (vol%)	Silicon (vol%)	Material	Initial porosity	Free carbon (vol%)	B_4C (vol%)[1]	SiC (vol%)	Silicon (vol%)
RI(P_1)[2]	20	80 ± 3	13 ± 1	7 ± 1	RIC(P_1)[2]	20	3 ± 0.5	80 ± 3	12 ± 1	8 ± 1
	30	70 ± 3	17 ± 1	13 ± 1		30	3 ± 0.5	70 ± 3	17 ± 1	13 ± 1
	40	60 ± 3	20 ± 1	20 ± 1		40	5 ± 0.5	60 ± 3	24 ± 1	16 ± 1
RI(P_5)[2]	20	80 ± 3	8 ± 1	12 ± 1	RIC(P_5)[2]	20	3 ± 0.5	80 ± 3	8 ± 1	12 ± 1
	30	70 ± 3	10 ± 1	20 ± 1		30	4 ±0.5	70 ± 3	9 ± 1	21 ± 1
	40	60 ± 3	12 ± 1	28 ± 1		40	6 ± 0.5	60 ± 3	10 ± 1	30 ± 1
RBM(P_75)[2]	25	84 ± 2	6 ± 1	10 ± 1	RB(P_5)[2]	30		69 ± 2	11 ± 1	20 ± 1

[1] Boron carbide: $B_4C + B_{12}(B,C,Si)_3$

[2] P_X is initial B_4C average particle size (mm).

the newly formed SiC phase. The second factor is related to initial particle size of B_4C. Amount of SiC in the final composite decreases with increasing initial particle size for a given process time. This feature is related to available B_4C surface for interaction with molten silicon, which is significantly higher for fine initial B_4C particles.

In the case of free-carbon addition to the green body prior to infiltration, amount of SiC that forms also strongly depends on initial porosity, with little influence from carbon addition. This "strange" fact may be related to thermodynamic equilibrium in the Si-B-C system for a given temperature. Free carbon "eats" some of the infiltrated silicon and leaves less silicon to interact with B_4C, resulting in less SiC formation from the Si–B_4C interaction. Data in Table 2 show that the total amount of SiC in RIC is very close to carbon-free samples (RI and RB), with similar particle sizes and initial porosity.

Another microstructural feature in this system that strongly depends on processing parameter is morphology of the newly formed SiC phase. In composites fabricated with free-carbon addition, SiC particles display a polygonal shape. For composites in which initial B_4C is the sole source of carbon, the SiC phase displays a platelike morphology. According to transmission electron microscopy analysis, the β-SiC phase always precipitates as single platelike particles from the silicon melt, preferably with the $\{111\}_\beta$ habit plane at the first stage. Available amount of carbon for SiC formation during the process stands behind the different morphology.

Pampuch et al.[13] and Ness and Page[14] discuss the mechanism of SiC formation in RBSC-based composites. At initial stages of the interaction, carbon is suggested to dissolve in the silicon melt, similar to a system without SiC particles.[15] This dissolution provides a gradient of carbon concentrations between the dissolution site and original SiC particles. Carbon diffuses to the surface of SiC particles, and newly formed SiC heterogeneously precipitates. These processes form the specific microstructure of RBSC composites (Figure 1). Moreover, Ness and Page[14] point out that formation of the β-SiC phase in RBSC composites starts as fingerlike particles, which transform to platelike shapes that then broaden to polygonal shapes.

In RBBC composites fabricated in the presence of free carbon, two carbon sources are available for SiC formation. Moreover, solubility of carbon in the silicon melt at equilibrium with SiC is extremely low and does not depend on carbon source. Nevertheless, in the vicinity of B_4C particles, conditions for SiC formation are different from those for free-carbon particles. Carbon and boron dissolve from B_4C particles into the silicon melt, and SiC and $B_{12}(B,C,Si)_3$ phases precipitate. The ternary carbide phase precipitates at the surface of original B_4C particles via a semicoherent interface and competes with SiC for carbon atoms.

SiC particles are nucleated within the melt only up to the stage at which dissolution of B_4C in the molten silicon

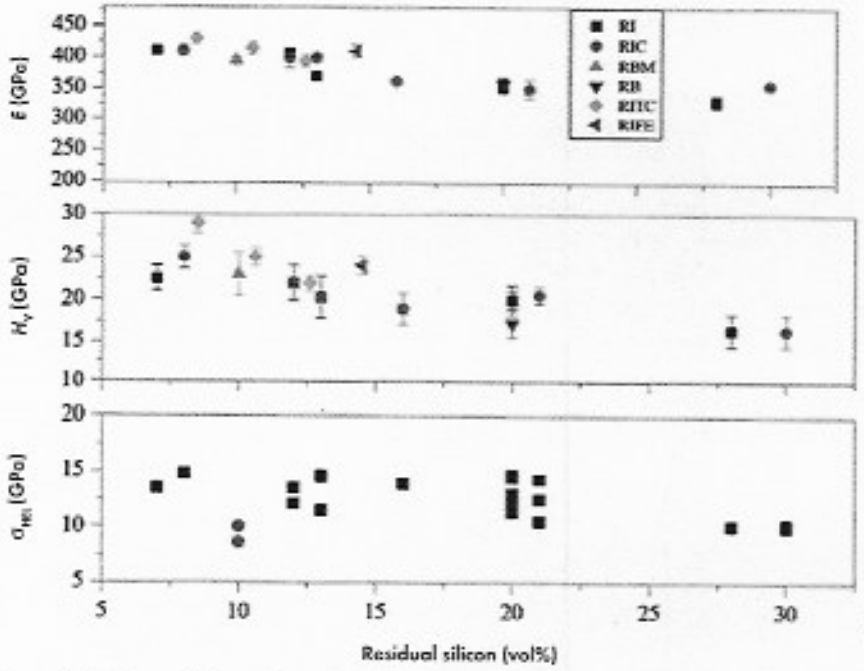


Figure 4. Elastic modulus, Vickers hardness, and σ_{HEL} of composites as a function of residual silicon.

Boron carbide-based armors: Problems and possible solutions

By Atta U. Khan, Vladislav Domnich, and Richard A. Haber

A critical assessment of recent advances in understanding of the nature and possible root causes of shear-induced amorphization in boron carbide for lightweight armor applications.

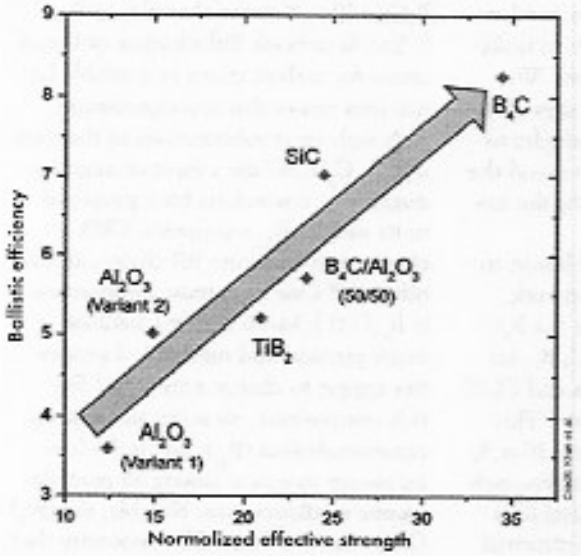


Figure 1. Relationship between ballistic efficiency against small arms ammunition and normalized effective strength for several armor ceramics.[2]

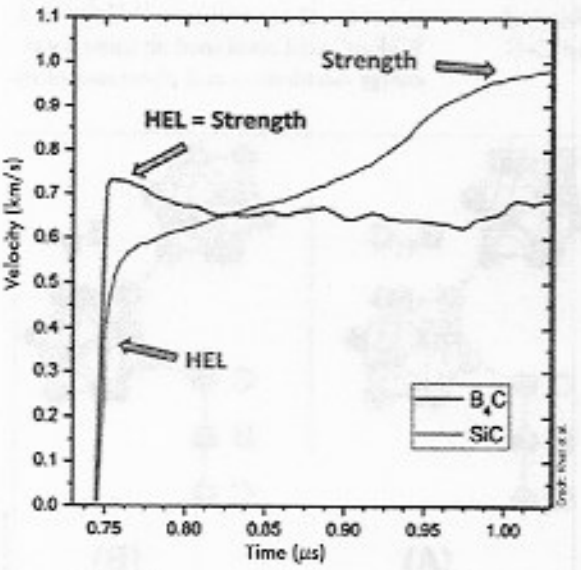


Figure 2. Shock wave profiles for commercial armor-grade B_4C and SiC ceramics measured with velocity interferometry diagnostics.[3] B_4C demonstrates postyield softening, which degrades its performance against high-density, high-velocity projectiles.

High hardness and low density make boron carbide (B_4C) an ideal candidate material for lightweight armor applications. Its yield strength in compression under dynamic uniaxial strain loading conditions, known as Hugoniot elastic limit (HEL), is on the order of 15–20 GPa[1]—higher than that observed in any other commonly used armor ceramic. With its high strength and low areal density, B_4C clearly outperforms other armor ceramics in ballistic testing involving small arms ammunition (Figure 1).[2]

However, quite unexpectedly, the ballistic efficiency of B_4C against high-density, high-velocity threats is inferior to many other armor ceramics. The literature links this observation to loss of shear strength in B_4C just above the HEL (Figure 2).[3] Whereas many other materials (e.g., silicon carbide (SiC)) become stronger well beyond the HEL, B_4C demonstrates glasslike fracture under these conditions.

In recent years, we have come to realize in the materials science and ballistic community that loss of shear strength might be related to formation of nanometer-sized amorphous bands when B_4C is subjected to certain critical strains under dynamic impact.[1,4] We believe that such shear-induced amorphous bands might act as nucleation sites for crack initiation, leading to ultimate fracture and fragmentation.[5] Whether or not amorphization is fully responsible for the abrupt degradation of B_4C under supercritical impact stresses, researchers clearly have demonstrated it occurs in ballistically impacted material and in material subjected to a variety of other contact loading situations, such as static and dynamic indentation, scratching, and machining.[1] Domnich et al.[1] provide an exhaustive overview of B_4C structure, properties, and amorphization.

Phase diagram and substitutional disorder

Scientists have debated the phase diagram of B_4C in general and the homogeneity region in particular for decades.[1] Elliott[6] used a

Capsule summary

TO PROTECT AND SERVE

Boron carbide is an ideal material for lightweight armor applications because of its high hardness and low density. Although the material is superior against small arms ammunition, its efficiency against high-density, high-velocity threats is low because of loss of shear strength.

MIX IT UP

Recent advances in understanding of shear-induced amorphization in boron carbide—particularly with computational efforts that imply possible amorphization mitigation in doped boron carbide—reveal renewed possibilities for boron carbide-based armor materials.

COMPOSITE POSSIBILITIES

Synthesis of composites of boron carbide with other potentially hard phases could reveal other deformation mechanisms involving secondary phases that suppress the amorphization problem, potentially resulting in a material with comparable or even higher hardness.

good starting point of very-high-purity boron (99.6%) and published the first detailed experimental phase diagram in 1961. However, Elliot ignored losses, although small, during arc melting. He took the existence of eutectic in annealed samples toward the carbon-rich end as an indication of maximum solubility of carbon in B_4C. Key points of this phase diagram (Figure 3) include a homogeneity range of 9.5–19.9-at.% carbon in B_4C and shifted composition of boron-rich eutectic very close to (B). Despite many other phase diagrams proposed since Elliott's original work, his remains the most reliable phase diagram and should be considered when dealing with the homogeneity region of B_4C.

Crystal structure of B_4C also is controversial, especially regarding location of carbon atoms in the lattice.[1] Extensive diffraction data in the literature have established that the basic building blocks in carbon-rich B_4C are an icosahedron and a three-atom chain, forming a rhombohedral $R\bar{3}m$ symmetry (Figure 4).[1] In general, boron forms covalent bonds. However, presence of only three valence electrons hinders the traditional 3-D network based on two-electron covalent bonds. Therefore, boron tends to make icosahedra comprising 12 atoms. We commonly refer to the lattice sites of the six atoms connecting the icosahedra to the end chain as equatorial sites and the remaining six atoms connecting the icosahedra as polar sites.

Based on the propensity of boron to form a 12-atom icosahedral network, researchers assumed early that the B_4C crystal structure was $(B_{12})CCC$, B_{12} for the 12-atom boron icosahedra and CCC for the three-atom carbon chain. This structure provides the necessary 20-at.% carbon concentration in the carbon-rich B_4C and retains a rhombohedral $R\bar{3}m$ symmetry. However, later experimental and modeling studies led to the conclusion that in carbon-rich B_4C, a carbon atom replaces one of the polar boron atoms in the unit cell, rendering the chain composition as CBC. Researchers currently widely accept that no C–C bonds are formed in B_4C.[1]

For more boron-rich compositions, the actual stoichiometry changes from B_4C (~20-at.% carbon) to almost $B_{10}C$ (~9-at.% carbon). Substitution of boron atoms for carbon atoms in available lattice sites causes this accommodation. Although exact substitutions in the starting $(B_{11}C_p)CBC$ are a topic of ongoing discussion, researchers have proposed units such as B_{12} icosahedra, CBB chains, and two-atom BB chains, among others.[1,7,8] One important composition is $B_{6.5}C$ (13.3-at.% carbon), because many physical and mechanical properties appear to change around it.[1] For this composition, ab initio simulations consistently find $(B_{12})CBC$ is the lowest energy structure among all possible atomic configurations. Notably, the $(B_{12})CBC$ structure has a $R\bar{3}m$ symmetry that is consistent with diffraction refinement data, whereas configurations that include a fixed position for carbon atoms in the icosahedra are inevitably reduced to a monoclinic symmetry.[1,9] Huhn and Widom[9] used combined ab initio total energy calculations and phenomenologi-

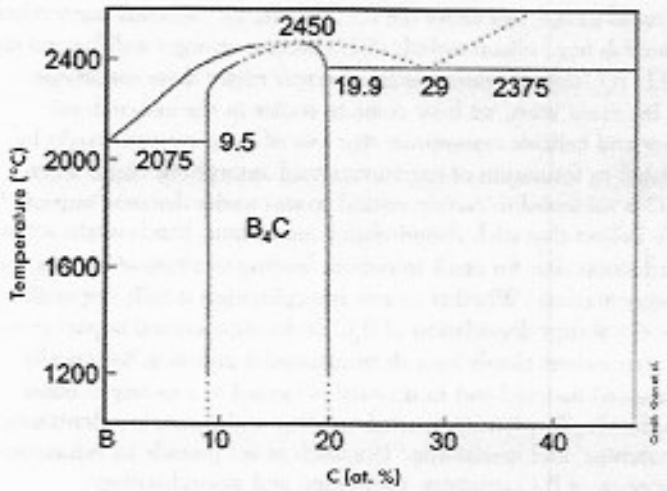


Figure 3. Phase diagram of B–C system reported by Elliott.[6] Because of use of high-purity boron, it is considered the most reliable phase diagram available.

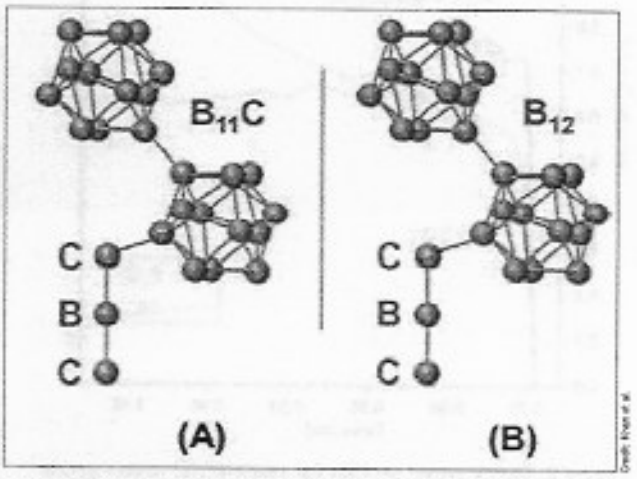


Figure 4. Principal structural units that comprise the crystal lattice of B_4C: 12-atom icosahedra and three-atom chains. Atomic configurations corresponding to (A) $B_{4.0}C$ and (B) $B_{6.5}C$ compositions. Note the random occupation of icosahedral polar sites by carbon atoms in (A), resulting in substitutional disorder.

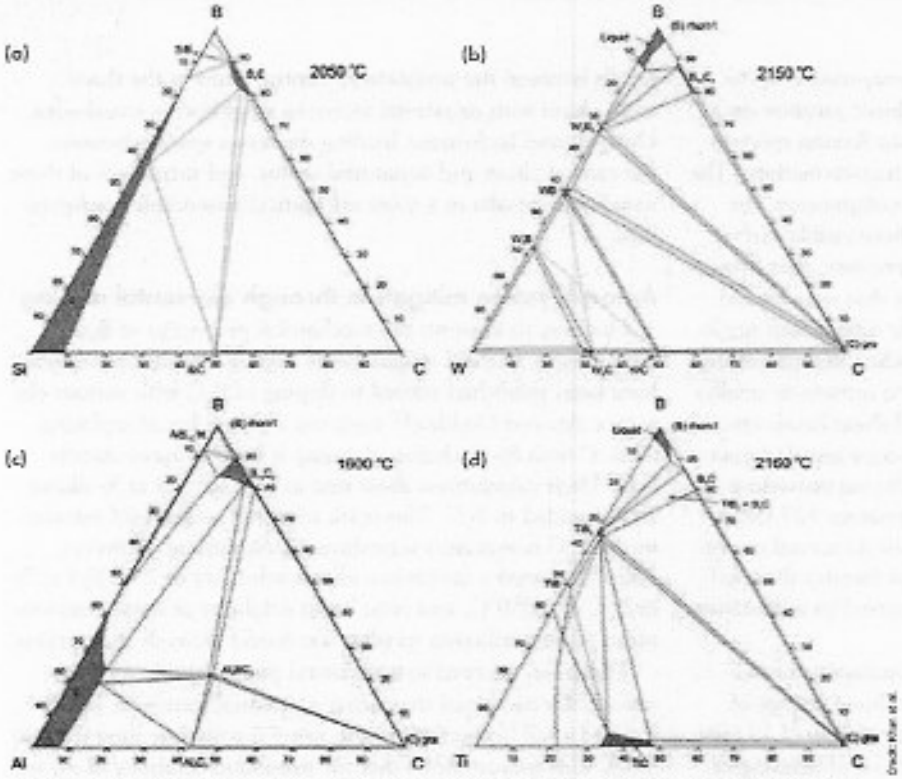


Figure 5. Phase diagrams of various ternary systems: (A) Si–B–C, reported by Telle,[21] where partial isothermal section is converted to a full section for better understanding using same tie lines; (B) W–B–C, reported by Rudy[22]; (C) calculated isothermal section of Al–B–C, reported by Lukas,[24] showing significant doping of silicon, tungsten, and aluminum, respectively; and (D) possible composite of B_4C–TiB_2.[25]

cal thermodynamic modeling to propose alternate carbon substitution in the six available icosahedron polar sites for a $(B_{11}C_p)CBC$ structure, which would then result in the average rhombohedral symmetry that is observed experimentally.

Such substitutional disorder may be an intrinsic property of B_4C, resulting in a nonzero configurational entropy even at 0 K (as in so-called geometrically frustrated systems).[10] This brings in question the validity of results of the majority of ab initio calculations, which consider stability of specific atomic configurations (often referred as polytypes or polymorphs) based on their total energy. Such calculations treat the material as a mixture of noninteracting polymorphs, thus neglecting configurational disorder.[1,11] Werheit[9] notes that no superlattice is known so far in B_4C. Therefore, we must assume that the differently composed elementary cells are randomly distributed. This situation is very different from the ideal crystal with a well-defined unit cell considered in a typical total energy minimization model.

Amorphization of B_4C under contact loading

Researchers have used high-resolution transmission electron microscopy (HRTEM) to observe formation of nanosized oriented amorphous bands in B_4C subjected to quasi-uniaxial compression, static indentation, dynamic indentation, scratching, and ballistic impact.[1] For indented areas and scratch debris, nanoscale bands coagulate and form larger amorphous zones.[1] Within the amorphous zone, nanosized grains of crystalline material with retained orientation might be present, indicating highly anisotropic deformation of B_4C under stress. In material recovered from plate impact experiments, there is no direct evidence of formation of amorphous material, although some groups interpret the available shock-loading data as indicative of a phase transformation or amorphization.[1,12] Finally, there is no experimental evidence that B_4C transforms to the amorphous state or experiences any type of phase transformation under hydrostatic compression up to 100 GPa.[1,13] Therefore, it is highly conceivable that shear stresses primarily drive amorphization of B_4C.

Ivashchenko et al.[14] theoretically addressed the nature of the amorphous phase using molecular dynamics methods. They showed that by stimulating amorphous B–C networks based on a 120-atom rhombohedral B_4C cell the amorphous phase consists of disordered icosahedra composed mainly of boron atoms connected by topologically disordered B–C and C–C networks. Experimentally, other researchers observed distorted icosahedra within amorphous bands by state-of-the art HRTEM techniques.[15]

Several groups have theoretically investigated the stability of various B_4C polytypes. Fanchini et al.[16] calculated total energies for various B_4C configurations under increasing hydrostatic pressure at room temperature. Their results indicate that the energetic barrier for pressure-induced amorphization of B_4C is lowest for the hypothetical $(B_{12})CCC$ polytype, which is unstable at 6–7 GPa during hydrostatic loading. The authors predict collapse of the $(B_{12})CCC$ structure to result in segregation of the (B_{12}) icosahedra and amorphous carbon in the form of 2–3-nm-wide bands along the (113) lattice direction, which favorably correlates with available TEM observations on indented and ballistically loaded samples. Therefore, according to this work, suppressing formation of the $(B_{12})CCC$ polytype during B_4C synthesis helps mitigate amorphization and improves ballistic efficiency against high-density, high-velocity threats.

However, validity of these calculations is highly debatable. Fanchini et al.[16] predict collapse of the $(B_{12})CCC$ polytype under compression at hydrostatic pressures of only 6–7 GPa, but available experimental data clearly demonstrate that the ambient phase of B_4C is stable under hydrostatic compression up to 100 GPa.[1,14] Moreover, there is a compelling evidence that C–C bonds are prohibited in B_4C. Therefore, a $(B_{12})CCC$ configuration should not exist in nature.[1]

Yan et al.[17] have emphasized the importance of taking into account nonhydrostatic stresses for understanding the stability of B_4C at high pressures. With a complete set of experiments

using quasi-hydrostatic and quasi-uniaxial compression up to 50 GPa followed by depressurization to ambient pressure on a B_4C single crystal, the authors engaged in situ Raman spectroscopy to detect possible high-pressure phase transformations. The authors found that under quasi-hydrostatic compression, the material remains a perfect single crystal without visible surface relief and cracking. After they released the pressure, they detected no evidence of amorphization in samples that were loaded hydrostatically. However, results significantly differ when single-crystal B_4C is subjected to quasi-uniaxial loading and unloading. In this case, depressurized samples break into numerous smaller fragments; evident cracks, surface relief, and shear bands are optically visible; and in situ Raman spectroscopy reveals formation of amorphous material at 13–16 GPa during unloading of samples that were previously loaded to pressures >25 GPa. Analysis of fully depressurized samples reveals nanosized oriented amorphous bands (HRTEM) and spectral features (Raman) typical for stress amorphized material as observed in indentation and scratching experiments.

The same group conducted theoretical simulations of uniaxial loading of B_4C that indicate a drastic volume change of the $(B_{11}C_p)$CBC unit cell at a destabilization pressure of 19 GPa (consistent with an HEL of 15–20 GPa) because of bending of the CBC chain.[17] They found that at higher loads, chain deformation continues until the $(B_{11}C_p)$CBC lattice is irreversibly distorted and that the central boron atom of the chain can bond with neighboring atoms in the icosahedra, forming a higher-energy structure. They propose that release of this energy during depressurization is responsible for collapse of the B_4C structure and formation of local amorphized bands.[17]

An et al.[18] further corroborated this conclusion using atomistic simulations when they found that the $(01\bar{1}\bar{1})/(\bar{1}101)$ slip system in $(B_{11}C_p)$CBC has the lowest shear strength and that this slip can lead to unique plastic deformation before failure in which a B–C bond between neighboring icosahedra breaks to form a carbon lone pair on the carbon atom within the icosahedron. Further shear leads this carbon atom to form a new bond with the boron atom in the middle of a CBC chain. This then initiates destruction of the icosahedron, leading to formation of a nanoscale amorphous band. As a remedy to mitigate amorphization in B_4C, An et al. propose to modify the B_4C synthesis processes to suppress formation of $B_{11}C_p$ icosahedra. They propose to achieve this result, in particular, by synthesizing more boron-rich B_4C, because they believed that $B_{11}C_p$ units are mostly replaced by B_{12} icosahedra for the $B_{6.5}C$ composition.

Calculations by Taylor et al.[19] determined that yield strength of the (B_{12})CBC configuration under shear strain is on the order of 30–40 GPa—about twice that of other structures involving carbon atoms in the icosahedron. This implies that $B_{6.5}C$ may be most stable under shear loading, further emphasizing the importance of investigating boron-rich boron carbides for possible mitigation of shear-induced amorphization and making material with improved ballistic performance. Similar to other modeling work,[17,18] Taylor et al. propose that softening of shear moduli is associated with formation of new bonds between the unsaturated central atom in the three-atom chain with equatorial atoms in neighboring icosahedra. Uniaxial and hydrostatic loading decreases spacing between the central chain and equatorial atoms, and formation of these new bonds results in a more energetically favorable configuration.

Amorphization mitigation through elemental doping

One way to improve the mechanical properties of B_4C, especially its fracture toughness, is doping. Numerous reports have been published related to doping of B_4C with various elements. An and Goddard[20] reported a possibility of replacing C–B–C with Si–Si chains, claiming it leads to more ductile B_4C. Their calculations show that as high as ~14 at.% silicon can be added to B_4C. This work triggered widespread interest in the B_4C community regarding silicon doping. However, Telle[21] reported a maximum silicon solubility of 2.5 ± 0.5 at.% in B_4C at 2,050°C, and even lower solubility at lower temperatures, in contradiction to what was found through simulations.

Therefore, we need to understand phase equilibria of this system. We converted the partial isothermal section of Telle's work to a full isothermal section using reported tie lines (Figure 5(A)). This section shows that the maximum solubility of silicon is around $B_{13}C_2$ composition. Telle also reports that silicon doping kicks carbon out of the B_4C lattice. In addition, silicon reacts with free carbon present in B_4C, detrimental to its hard-



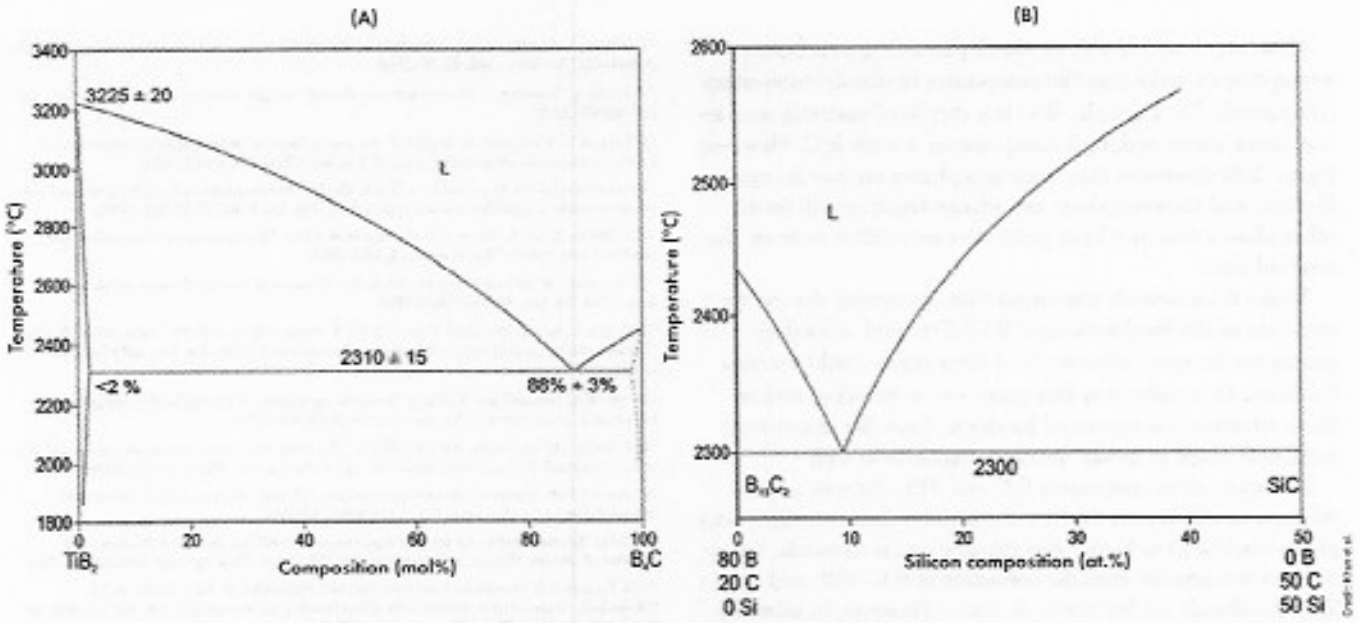


Figure 6. Pseudo-binary phase diagram of (A) TiB_2–B_4C as reported by Rudy and Windsch[25] and (B) B_4C–SiC as reported by Secrist,[26] indicating eutectics.

ness, and converts it to a more desirable SiC. Most often, B_4C is sintered by using either spark plasma sintering (SPS) or uniaxial hot pressing at ~2,050°C ± 150°C. Therefore, we conclude that, at least with these two techniques, maximum solubility of silicon in B_4C cannot be achieved. Instead, silicon solubility remains close to the reported 2.5 ± 0.5 at.%. However, we can realize higher silicon doping using other techniques, such as arc melting, where the temperature usually is much higher. However, no one has reported higher silicon solubility yet.

The aforementioned report by An and Goddard[21] regarding the possible impact of silicon doping on fracture toughness inspires us to consider other doping elements. Encouraged by that possibility, we briefly summarize here a few potential doping elements based on reported phase diagrams. Figures 5(B) and 5(C) illustrate considerable solubility of tungsten and aluminum in B_4C. Although we have not theoretically evaluated the effect of these elements, they might present similar results. Additionally, presence of aluminum melt in equilibrium with B_4C suggests that we can use this liquid as a sintering aid for B_4C and help sinter this material at lower temperatures. Among all experimental or calculated published ternary systems, aluminum shows the highest amount of doping in B_4C and may significantly change fracture toughness, hardness, etc. Moreover, a different B/C ratio would result in a different amount of dopants.

Although there is very low solubility of titanium in B_4C (Figure 5(D)), combined doping of titanium and zirconium is effective in improving hardness, compressive strength, and impact elasticity of B_4C.[22] Presumably, improved impact elasticity is associated with an increase of free electrons from the doped metal atoms, while preserving the covalent bonding responsible for high hardness—and resulting in retained hardness. Therefore, multiple doping elements at the same time could be a route to a less amorphized and harder B_4C with better elastic response to ballistic impact. Generally, we observe maximum solubility around a $B_{11}C_2$ composition for almost all doping elements. In addition, higher boron content as compared with B_4C might better resist amorphization, although hardness may decrease.[19] Therefore, we should target doping around a $B_{13}C_2$ composition.

Moreover, the low atomic weight of magnesium makes it an interesting candidate for B_4C doping. Recent experiments in our laboratory indicate a significant amount of magnesium doping in B_4C, and we observed no considerable oxidation of this sintered material. However, we are evaluating its effect on mitigation of amorphization, fracture toughness, and hardness.

Improving ballistic efficiency through composites

One way that we circumvent the amorphization problem in B_4C is to make composites. We believe that amorphized bands are responsible for crack initiation and growth and that secondary phases may hinder these cracks, preventing the material from failure. However, we recognize that there are certain prerequisites to meet before considering a composite. One of the most important parameters is a comparable hardness of the second phase. In addition, overall density of the composite should not exceed that in conventional armor materials. Further, armors in general and body armors in particular should be lightweight. Figure 5(D) shows that B_4C and TiB_2 are in thermodynamic equilibrium at 2,160°C, which is close to the general sintering temperature of B_4C.

TiB_2 also has high hardness. Therefore, its composites could be possible armor materials. Although TiB_2 has a rather high density, around 10 wt.% of it could be used to result in an overall density of <3 g/cm³, well within the acceptable limits for body armors. ZrB_2 or HfB_2 also lie in thermodynamic equilibrium with B_4C, but their high density hinders use as a composite material. Moreover, the hardness of these materials is comparable to TiB_2, but their prices are generally higher than TiB_2. Therefore, it is not worth considering these two compounds for armors.

However, it is desirable to check phase diagrams before attempting to make possible composites of various interesting compounds. For example, WC is a very hard material, and we may think about making a composite of it with B_4C. However, Figure 5(B) illustrates that these two phases are not in equilibrium, and sintering these two phases together will form other phases that may have properties very different from the targeted ones.

It also is immensely important that we control the microstructure of the final materials. Well-dispersed secondary phases are far more effective, and finer grains could increase hardness. Generally, very fine grain size of eutectics makes them attractive for improved hardness. Lamellar microstructures may result in better fracture toughness as well.

A eutectic exists comprising B_4C and TiB_2. Eutectic microstructure in addition to the intrinsic high hardness of constituent phases could lead to harder and stronger armor materials. Figure 6 shows two possible eutectics consisting of B_4C–TiB_2 and B_4C–SiC. We already use SiC for body armor. However, its relatively high density and rather lower hardness make it vulnerable to emerging threats. SiC composites with B_4C and, more importantly, eutectic microstructure with B_4C holds promise and may overcome the intrinsic problems of standalone B_4C or SiC.

Acknowledgments

The authors thank Chawon Hwang of Rutgers University for insightful discussions. This research was sponsored by the Army Research Laboratory under Cooperative Agreement No. W911NF-12-2-0022, the Defense Advanced Research Projects Agency under Grant No. W31P4Q-13-1-0001, and the National Science Foundation I/UCRC Directorate under Award No.1540027.

About the authors

Atta U. Khan, Vladislav Domnich, and Richard A. Haber are with the Department of Materials Science and Engineering at Rutgers University (Piscataway, N.J.). Contact Haber at rich.haber@rutgers.edu.

References

[1]V. Domnich, S. Reynaud, R.A. Haber, and M. Chhowalla, "Boron carbide: Structure, properties, and stability under stress," *J. Am. Ceram. Soc.*, 94 [11] 3605–28 (2011).

[2]Z. Rosenberg and Y. Yeshurun, "The relation between ballistic efficiency and compressive strength of ceramic tiles," *Int. J. Impact Eng.*, 7 [3] 357–62 (1988).

[3]D.E. Grady and R.L. Moody, "Shock compression profiles in ceramics," Report No. SAND960551, Sandia National Laboratories, Albuquerque, N.M., 1996.

[4]Q. An, K.M. Reddy, J. Qian, K.J. Hemker, M.W. Chen, and W.A. Goddard III, "Nucleation of amorphous shear bands at nanotwins in boron suboxide," *Nat. Commun.*, 7, 11001 (2016).

[5]Q. An and W.A. Goddard, "Atomistic origin of brittle failure of boron carbide from large-scale reactive dynamics simulations: Suggestions toward improved ductility," *Phys. Rev. Lett.*, 115 [10] 105501 (2015).

[6]R.F. Elliott, "The boron-carbon system," Report No. ARF-2200-12, Armour Research Foundation, Illinois Institute of Technology, Chicago, Ill., 1961.

[7]O. Sologub, Y. Michiue, and T. Mori, "Boron carbide, $B_{1-y}C_{1+y}$ (δ = 0.12, γ = 0.01)," *Acta Crystallogr. E*, 66 [8] i67 (2002).

[8]H. Werheit, "Boron carbide: Consistency of components, lattice parameters, fine structure, and chemical composition makes the complex structure reasonable," *Solid State Sci.*, 60, 45–54 (2016).

[9]W.P. Hsieh and M. Widom, "A free-energy model of boron carbide," *J. Stat. Phys.*, 150 [3] 452–91 (2013).

[10]K. Shirai, K. Sakurai, and N. Uemura, "Theoretical study of the structure of boron carbide $B_{13}C_2$," *Phys. Rev. B*, 90 [6] 064109 (2014).

[11]C. Kurdas, A. Awarkh, and G. Subhash, "Crystallographic and spectral equivalence of boron-carbide polymorphs," *Sci. Mater.*, 122, 82–85 (2016).

[12]D.E. Grady, "Hugoniot equation of state and dynamic strength of boron carbide," *J. Appl. Phys.*, 117 [16] 165904 (2015).

[13]F. Dove, M.H. Mangham, A. Hashaz, T. Ho, and S. Thatcher, "New insights into the enigma of boron carbide inverse molecular behavior," *J. Solid State Chem.*, 215, 85–93 (2014).

[14]V.L. Solozhenko, V.Z. Shevchenko, and P.E.A. Turchi, "First-principles study of the atomic and electronic structures of crystalline and amorphous B_4C," *Phys. Rev. B*, 80 [23] 235208 (2009).

[15]K.M. Reddy, P. Liu, A. Hirata, T. Fujita, and M.W. Chen, "Atomic structure of amorphous shear bands in boron carbide," *Nat. Commun.*, 4, 2483 (2013).

[16]G. Fanchini, J.W. McCauley, and M. Chhowalla, "Behavior of disordered boron carbide under stress," *Phys. Rev. Lett.*, 97 [3] 035502 (2006).

[17]C.Q. Yan, Z. Tang, L. Zhang, J.J. Guo, C.Q. Jin, Y. Zhang, T. Goto, J.W. McCauley, and M.W. Chen, "Depressurization amorphization of single-crystal boron carbide," *Phys. Rev. Lett.*, 102 [7] 075505 (2009).

[18]Q. An, W.A. Goddard, and T. Cheng, "Atomistic explanation of shear-induced amorphous band formation in boron carbide," *Phys. Rev. Lett.*, 113 [9] 095501 (2014).

[19]D.E. Taylor, J.W. McCauley, and T.W. Wright, "The effects of stoichiometry on the mechanical properties of icosahedral boron carbide under loading," *J. Phys.: Condens. Matter.*, 24 [50] 505402 (2012).

[20]Q. An and W.A. Goddard, "Microalloying boron carbide with silicon to achieve dramatically improved ductility," *J. Phys. Chem. Lett.*, 5 [23] 4169–74 (2014).

[21]R. Telle, "Structure and properties of Si-doped boron carbide", pp. 249–67 in *The Physics and Chemistry of Carbides, Nitrides, and Borides*, Vol. 185. Edited by R. Freer. Springer, Netherlands, 1990.

[22]Z.D. Kovziridze, Z. Mestvirishvili, G. Tsiskarishvi, N.S. Nitharadze, M. Mshvildadze, and E. Nikoleishvili, "Improvement of boron carbide mechanical properties in B_4C–TiB_2 and B_4C–ZrB_2 systems," *J. Electron. Cool. Therm. Contr.*, 3, 45–48 (2013).

[23]E. Rudy, "Experimental phase equilibria of selected binary, ternary, and higher-order systems. Part V. The phase diagram W-B-C," Report No. AFML TR 69-117 Part 5, Air Force Materials Laboratory, Wright-Patterson Air Force Base, Ohio, 1970.

[24]H.L. Lukas, *Constitution of Ternary Alloys*, Vol. 3, pp. 140–46. Edited by G. Petzow and G. Effenberg. VCH, Weinheim, Germany, 1990.

[25]E. Rudy and S. Windisch, "Ternary phase equilibria in transition-metal-boron-carbon-silicon systems. Part II. Ternary systems. Vol. XIII. Phase diagrams of the systems Ti-B-C, Zr-B-C, and Hf-B-C," Report No. AFML-TR-65-2, Air Force Materials Laboratory, Wright-Patterson Air Force Base, Ohio, 1966.

[26]D.R. Secrist, "Phase equilibria in the system boron carbide-silicon carbide," *J. Am. Ceram. Soc.*, 47 [3] 127–30 (1964). ■

